The detrimental invasiveness of glioma cells controlled by gadolinium chelate-coated gold nanoparticles

Maxime Durand, Elodie Lelièvre, Alicia Chateau, Alexandre Berquand, Gautier Laurent, Philippe Carl, Stephane Roux, Lise Chazée, Rana Bazzi, Frédéric Eghiaian, et al.

Nanoscale

Accepted Manuscript

This article can be cited before page numbers have been issued, to do this please use: M. Durand, E. Lelièvre, A. Chateau, A. Berquand, G. Laurent, P. Carl, S. Roux, L. Chazée, R. Bazzi, F. Eghiaian, P. Rondé, J. Jubréaux, M. Barberi-Heyob, P. Chastagner, J. Devy and S. Pinel, *Nanoscale*, 2021, DOI: 10.1039/D0NR08936B.

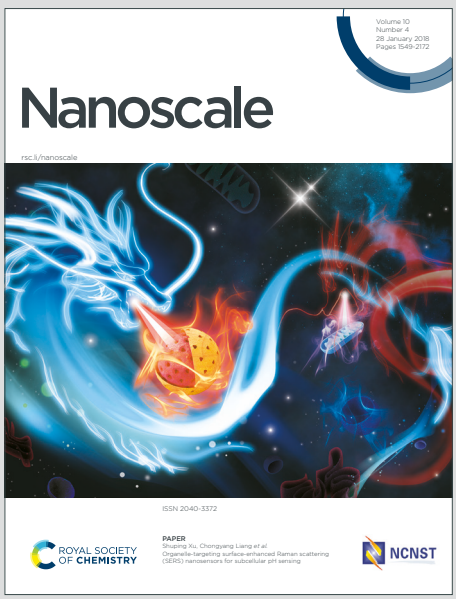

ROYAL SOCIETY OF CHEMISTRY

rsc.li/nanoscale

View Article Online
DOI: 10.1039/D0NR08936B

TITLE

THE DETRIMENTAL INVASIVENESS OF GLIOMA CELLS CONTROLLED BY GADOLINIUM CHELATE-COATED GOLD NANOPARTICLES

Authors

Maxime DURAND[1], Elodie LELIEVRE[2], Alicia CHATEAU[1*], Alexandre BERQUAND[4*], Gautier LAURENT[3], Philippe CARL[5], Stéphane ROUX[3], Lise CHAZEE[2], Rana BAZZI[3], Frederic EGHIAIAN[6], Justine JUBREAUX[1], Philippe RONDE[5], Muriel BARBERI-HEYOB[1], Pascal CHASTAGNER[1], Jérôme DEVY[2‡], Sophie PINEL[1‡]

[1]Université de Lorraine, CNRS, CRAN, F-54000 Nancy, France

[2]Université de Reims-Champagne-Ardennes, UMR CNRS/URCA 7369, MEDyC, F-51100 Reims, France

[3]Université Bourgogne Franche-Comté, UMR CNRS 6213-UBFC, UTINAM, F-25000 Besançon, France

[4]Université de Reims-Champagne-Ardennes, EA 4682, F-51100 Reims, France

[5]Université de Strasbourg, CNRS UMR 7021 – Strasbourg, France.

[6] Abberior Instruments GmbH, F-13008 Marseille

*These authors contributed equally

‡These authors contributed equally

Corresponding authors

Sophie Pinel: sophie.pinel@univ-lorraine.fr and Jérôme Devy: jerome.devy@univ-reims.fr

Conflict of interest

The authors declare no competing financial interests.

Author contributions

M. DURAND, E. LELIEVRE, A. CHATEAU, L. CHAZEE & J. JUBREAUX: *in vitro* biological experiments and data analysis.

A. BERQUAND: AFM experiments and data analysis.

G. LAURENT, S. ROUX & R. BAZZI: Synthesis and characterization of nanoparticles.

F. EGHIAIAN: STED microscopy experiments and data analysis.

P. CARL & P. RONDE: traction force microscopy experiments and data analysis.

M. BARBERI-HEYOB & P. CHASTAGNER : scientific & clinic discussion.

J. DEVY & S. PINEL: project management and coordination, data analysis and manuscript redaction.

View Article Online
DOI: 10.1039/D0NR08936B

ABSTRACT

Glioblastoma are characterized by an invasive phenotype, which is thought to be responsible for recurrences and the short overall survival of patients. In last decade, the promising potential of ultrasmall gadolinium chelate-coated gold nanoparticles (namely Au@DTDTPA(Gd)) was evidenced for image-guided radiotherapy in brain tumors. Considering the threat posed by invasiveness properties of glioma cells, we were interested to further investigate the biological effects of Au@DTDTPA(Gd) by examining their impact on GBM cell migration and invasion. In our work, exposure of U251 glioma cells to Au@DTDTPA(Gd) led into high accumulation of gold nanoparticles, that were mainly diffusely distributed in the cytoplasm of the tumor cells. Experiments pointed out a significant decrease in glioma cells invasiveness when exposed to nanoparticles. As the proteolysis activities were not directly affected by the intracytoplasmic accumulation of Au@DTDTPA(Gd), the anti-invasive effect cannot be attributed to a matrix remodeling impairment. Rather, Au@DTDTPA(Gd) nanoparticles affected the intrinsic biomechanical properties of U251 glioma cells, such as cell stiffness, adhesion and generated traction forces, and significantly reduced the formation of protrusions, thus exerting an inhibitory effect on their migration capacities. These results highlight the interest of Au@DTDTPA(Gd) nanoparticles for the therapeutic management of astrocytic tumors, not only as radio-enhancing agent but also by reducing invasive potential of glioma cells.

Keywords: Gold nanoparticles, migration, invasion, biomechanical properties, glioblastoma

View Article Online
DOI: 10.1039/D0NR08936B

INTRODUCTION

Glioblastoma (GBM) is the most aggressive, deadliest, and most common brain malignancy in adults. GBM is characterized by an invasive phenotype, which enables tumor cells to infiltrate into surrounding brain tissue. GBM tumor cells invade healthy brain and migrate along Scherer's structures, including pre-existing blood vessels, white matter tracts and the subarachnoid space. The highly migratory capability of these tumor cells is thought to be responsible for the short overall survival of GBM patients, since infiltrative cells always remain following cytoreductive surgery and lead to recurrence. Unfortunately, several experimental converging clues suggest that migration/invasion abilities of glioblastoma cells could be enhanced by therapeutic intervention such as surgical excision or irradiation[1]

In a recent review, we presented how the rapid development of nanomedicine for cancer applications opens up new perspectives for GBM therapy and imaging-guided treatments. Among promising innovation, many preclinical studies are ongoing and investigate the potential of gold nanoparticles as drug delivery system, to enhance external beam radiotherapy or to induce photothermal ablation[2]. The lack of significant cell toxicity in a wide concentration range may explain the craze for the use of gold nanoparticles (AuNPs) in cancer therapies. In this therapeutic context, gold nanoparticles with a diameter smaller than 10 nm should be preferred because (i) they can be eliminated by renal clearance which is a pre-requisite to the *in vivo* application of non-biodegradable nanoparticles[3] (ii) and they are more efficient than large nanoparticles for enhancing the radiation dose effect[4] . In accordance with these prerequisites, Roux's research group has developed ultrasmall polyaminocarboxylate-coated gold nanoparticles, namely Au@DTDTPA, that exhibit a promising potential for image-guided radiotherapy for brain tumors. Au@DTDTPA nanoparticles behave as positive contrast agents for magnetic resonance imaging (MRI) and as radiotracers for nuclear imaging (planar scintigraphy and single photon emission computed tomography (SPECT)) when they are labeled by Gd^{3+} and $^{99m}Tc^{4+}$ or $^{111}In^{3+}$ ions, respectively. After intravenous injection, authors showed that these nanoparticles are removed from the body mainly by renal excretion. Further, X-rays irradiation 5-10 minutes after intravenous administration of Au@DTDTPA(Gd) increased the life span of rats bearing brain tumor by a factor 2 in comparison to animals treated only by radiotherapy[5]

Despite the lack of major toxicity of gold nanoparticles, some articles have reported that AuNPs internalization by cells can affect cell proliferation, migration and invasion, alter metabolic activity, and reprogram secretome. For example, Pernodet *et al.* found that actin stress fibers disappeared and properties such as cell spreading, cell adhesion, and cell growth were altered dramatically as a result of intracellular gold nanoparticles presence in human dermal fibroblasts[6]. Similarly, gold nanoparticles seem to be able to reduce tumor growth and metastasis[7,8].

Knowing that migrating cells remain a major threat for glioblastoma-bearing patients, these recent data about AuNPs led us to further investigate the potential of Au@DTDTPA(Gd) and to examine their effects on GBM cell migration and invasion. Glioma cell invasion is a complex multi-step biological process that is regulated by an integrated network of biochemical and biomechanical events, involving many changes in morphological and adhesion properties and microenvironment remodeling. In this context, different *in vitro* approaches such as 3D spheroids tumor invasion assays, scratch assay and cell tracking by time lapse videomicroscopy, traction force

microscopy or atomic force microscopy, allowed us to get more insight into migration/invasion properties of glioblastoma cells when exposed to Au@DTDTPA(Gd) nanoparticles.

View Article Online
DOI: 10.1039/D0NR08936B

RESULTS AND DISCUSSION

Au@DTDTPA(Gd) nanoparticles uptake and consequences on cell viability and proliferation

In the past two decades, many studies have demonstrated that the cellular uptake depends on nanoparticles size, shape and coating[9–11]. The cellular accumulation of gold nanoparticles was time- and concentration dependent until a steady-state[9–11] and quantitative and qualitative distribution appeared as a key parameter that affects direct cytotoxicity and therapeutic activity such as radiosensitizing potential[12,13]. Hence, the first step aimed at quantifying the intracellular gold after glioma cells exposition to Au@DTDTPA(Gd) and evaluating consequences on cell viability and proliferation.

Elemental Au quantification by inductively coupled plasma mass spectrometry (ICP-MS) revealed that after 24h of exposure, Au quantity accumulated into U251 cells was similar regardless of the concentration of nanoparticle used (1 and 5 mM). Uptaken Au@DTDTPA(Gd) nanoparticles reached about 6.10^5 to 7.10^5 per cells (Table 1). STED microscopy experiments were conducted using Cyanine3-labeled Au@DTDTPA(Gd) and markers of particular compartments (*i.e.* antibodies directed against EEA1 for endosomes, calnexin for rough endoplasmic reticulum, vinculin for focal adhesion complexes and CoxIV for mitochondria (Figure 1A-1D)), to precise subcellular distribution of nanoparticles. Nanoparticles strongly accumulate in the cytoplasm as a diffuse pattern, while fluorescence is also observable into punctate structures at the periphery of the nucleus (Figure 1E). Surprisingly, we did not notice small or large clusters of nanoparticles in cytoplasmic vesicles such as endosomes nor in focal adhesion complexes. The ultrasmall size of Au@DTDTPA(Gd) nanoparticles and the lack of endosome/lysosome-confined intracellular clusters render nanoparticles undetectable with the usually used transmission emission microscopy. Similarly, Huang *et al.* have synthetized 2 nm, 6 nm and 15 nm-sized gold nanospheres and used tiopronin, a pharmaceutical drug including a thiol group, as a stabilizing agent. The authors quantified 5.10^5 to 5.10^6 nanoparticles/cell in a breast cancer monolayer model and they showed that the 2 and 6 nm AuNPs were mostly localized in the cytoplasm without any aggregation and also about 15% were able to enter the nucleus[11]. Afterwards, Boyoglu *et al.* confirmed that 3 nm and 10 nm AuNPs are efficient in entering the cytoplasm and nucleus of Hep-2 cells[14].

Even if gold materials are generally considered to be bio-inert, nontoxic and biocompatible, nanoscale gold particles may have much higher bioactivity due to their increased “surface area to volume ratio” that can result in direct cytotoxicity. Induction of apoptosis, cell cycle delay or generation of reactive oxygen species were described as potential cytotoxic effects of gold nanoparticles, according to their physicochemical properties[15,16].

With 97% cell viability following 24 h exposure, no direct toxic effects were noticed on U251 cells despite the strong internalization of nanoparticles in cancer cells (Figure 1F). When the global behavior of U251 glioma cells was followed for 70h with a cell-impedance measurement system (xCELLigence real-time cell analysis system), no alteration was noticed for nanoparticles-treated cells (data not shown). Using flow cytometry, we also investigated the influence of gold nanoparticles on cell cycle distribution and the proliferation index (*i.e.* percent S phase + percent G2/M phase) was calculated as previously described[17]. Sixteen hours after removal of Au@DTDTPA(Gd) nanoparticles, the proliferation index of U251 glioma cells treated with gold nanoparticles was unchanged as compared to untreated cells (Supporting Information SI1).

Collectively, our results indicate that the concentrations of the Au@DTDTPA(Gd) nanoparticles used in this study are lower than those affecting viability and proliferation of U251 glioblastoma cells.

Au@DTDTPA(Gd) nanoparticles reduced invasion abilities of glioma cells

Both in patients and *in vitro* models, glioblastoma cells are well-known to exhibit a highly invasive behavior leading in diffuse infiltration of surrounding[18]. To explore and decipher the mechanisms developed by invading cells in glioblastoma, the invasive behavior of the U251 cell line was extensively studied using a variety of methods and materials to mimic the *in vivo* microenvironment (2D or 3D extracellular matrix, organotypic slice). Multicellular tumor spheroids embedded in a 3D matrix represent invaluable tools to analyze cell invasion and to mimic cancer microenvironment[19,20]. We have investigated the impact of Au@DTDTPA(Gd) nanoparticles on invasive capacities of U251 cells. For that purpose, U251 spheroids were exposed to 1 and 5 mM of Au@DTDTPA(Gd) nanoparticles for 24 h and then, embedded in a matrix mixing Matrigel® and hyaluronic acid. As recently published, we have previously confirmed that Au@DTDTPA(Gd) nanoparticles were able to diffuse and be distributed throughout the spheroids, reaching the center of the tumor[21]. Figure 2 shows representative images of U251 spheroids in their 3D matrix 4 days post-seeding. While the dark areas correspond to spheroids' cores including necrotic, quiescent and proliferative cells, we can notice the cells on the edge that radially extend into the matrix (Figure 2A). Some of them seem to move individually (black arrows) while other organized in clusters (denser areas) suggest collective cell motion (white arrows) (Figure 2B). To assess the effect of Au@DTDTPA(Gd) nanoparticles on U251 invasiveness, spheroid initial/end sizes and invasiveness area were determined. With or without exposure to nanoparticles, the central core similarly grew during the culture to reach the mean final size of 0.516 ± 0.028 mm², 0.420 ± 0.076 mm² and 0.494 mm² ± 0.026 mm² for untreated-, 1 mM and 5 mM nanoparticles-treated spheroids, respectively. As shown in Figure 2C, the invasion capacities of the U251 cells pretreated with Au@DTDTPA(Gd) were approximately 20-25% lower than those of the control cells: invasion distances and invasion areas reached respectively, 820 ± 16 µm and 3.570 ± 0.135 mm² for untreated control spheroids ; 644 ± 14 µm and 2.719 ± 0.154 mm² for 1 mM nanoparticles-treated spheroids *($p < 0.005$ vs Ctrl);* 678 ± 21 µm and 2.899 ± 0.147 mm² for 5 mM nanoparticles-treated spheroids *($p < 0.005$ vs Ctrl)*. Thus, 3D invasion assays revealed a significant inhibitory effect of our ultrasmall gold nanoparticles on invasive capacities for U251. Inhibitory effects were previously described by Zhou *et al.* for breast, prostate and melanoma cancer cells exposed to gold nanorods using transwell invasion assays[22]. Similarly, Au@Pt nanoseeds have been shown to reduce invasiveness of kidney cancer cells in Boyden chambers[23].

To overcome the structural restraints of brain tissue organization, invading glioma cells need remarkable plasticity and proteolytic activity allowing them to move through the brain parenchyma, along the blood vessels and white matter tracks[24]. In this context, we were interested in studying the impact of Au@DTDTPA(Gd) uptake in a first step, on proteolysis abilities of U251 cells and in second step, on intrinsic cell plasticity and motility.

Impact of Au@DTDTPA(Gd) nanoparticles uptake on proteolytic activity and on glioma cell motility

Matrix metalloproteinases (MMPs) like serine proteases urokinase plasminogen activators constitute the main groups of proteases capable of degrading extracellular matrix proteins (fibronectin, type IV-collagen, proteoglycan…) and involved in GBM growth and dissemination. A strong correlation exists between elevated

View Article Online
DOI: 10.1039/D0NR08936B

levels of urokinase plasminogen activators (uPA) and MMPs with cancer progression, metastasis and shortened patient survival[25].

Concerning the MMPs family, gelatinases MMP-2 and MMP-9 and the membrane-type MT1-MMP are found to be expressed by glioma cells and already described for their contribution in tumor progression[26]. Moreover, a previous study has demonstrated a downregulation of MMP-2 and -9 expression after the exposure of papillary thyroid carcinoma cells to 10 nm AuNPs at a dose of 50 µg/mL[27]. Thus, we explored the consequences of Au@DTDTPA(Gd) on metalloprotease expression and activity. RT-qPCR analysis indicated that U251 cells expressed MT1-MMP, MMP-2, but not MMP-9. Exposure to Au@DTDTPA(Gd) induced a slight but not significant decrease in MT1-MMP and MMP2 mRNA levels. Using gelatin zymography method, we focused on proteolytic activity of gelatinases. In accordance with others[28], we did not detect any gelatinolytic activity of MMP-2 nor MMP-9 in conditioned media of U251 cells, even in untreated samples. MT1-MMP analysis was performed by using a biotinylation approach in order to only recover active MT1-MMP at the cell membrane. Proteolytic activity of MT1-MMP was found in untreated U251 at the same level as after Au@DTDTPA(Gd) nanoparticles uptake (Supporting Information SI2).

Thus, the MMPs do not seem to be involved in the reduced invasive capabilities of U251 cells treated by NPs. The plasminogen/plasmin system is another system well described for its involvement in the extracellular matrix degradation during GBM progression[29]. Notably, the serine protease urokinase plasminogen system (uPA, uPAR) participates actively to ECM restructuring through plasmin and MMPs activation. Our preliminary analyses using RTqPCR on cell lysate and proteome arrays on conditioned media did not show noteworthy influence of NPs on the plasminogen/plasmin system (data not shown).

While the reduced abilities of invasion of U251 after Au@DTDTPA(Gd) endocytosis cannot be directly explained by an interference of the nanoparticles with the proteolysis processes, we questioned whether the nanoparticles can affect the migration capabilities of glioma cells. Glioblastoma cells show a versatile repertoire of migration modes, allowing them to adapt their strategies in response to changing environmental conditions. Indeed, these tumor cells can exhibit individual (amoeboid or mesenchymal) or collective migration modes, depending on the local properties of the extracellular matrix[30]. In this regard, different tests were carried out to evaluate the effects of Au@DTDTPA(Gd) on migration capacities of U251 cells.

A scratch assay which is considered as the standard *in vitro* technique was firstly performed for probing collective cell migration in two dimensions[31] . Images were captured immediately (0 h) and 16 h after the scratch and surface of the healing wound was determined using imageJ software (Figure 3A). At the end point of experiment, the healing area reached 33% for the control. After exposure to nanoparticles, the recovery of the wounding area was only 15%, *i.e.* 2 times less than in the control samples (Figure 3B).

Then, time-lapse videomicroscopy and cell tracking experiments were performed on monodispersed cells to estimate cells velocity and directionality. While traditional methods rely on the Boyden chamber migration assays to measure individual migration in response to chemotactic signals, we preferred time-lapse videomicroscopy because it allows the measurement of individual migration parameters and the visualization of morphological changes that cell undergoes during migration[32]. In untreated U251 cells, movies revealed a

repeated sequential polarized apparition of enlarged lamellipodia associated to cell polarity and directional displacement of cells with typical mesenchymal morphologies (Movie 1 left).

Looking at each cell individually, exposition to Au@DTDTPA(Gd) seem to interfere with cell polarity establishment as we observed a fast turnover of lamellipodia in any direction that leads to both reduced directional displacement and reduced apparent velocity (Movie 1 right). Indeed, cell tracking quantification revealed that U251 cells seeded onto fibronectin exhibit a velocity of 0.72 ± 0.02 µm/min and the traveled distance reached 1050 ± 31 µm/24 h. U251 cell motility rates was significantly altered after nanoparticles endocytosis, because U251 cell velocity was decreased by 43% (0.39 ± 0.02 µm/min), the traveled distance by 45% (581 ± 26 µm/24 h) and directional cell migration (Euclidian distance) by 65% compared to untreated cells (Figures 3C-E).

Together, these results indicate that Au@DTDTPA(Gd) can exert a significant inhibitory effect on both collective and individual migration of U251 cells. Our specific observations for the Au@DTDTPA(Gd) nanoparticles can probably be generalized to most of gold nanoobjects. Indeed, several previous studies using wound healing assay or transwelll chamber have reported that gold nanospheres and gold nanorods, regardless of their size, their concentration or the cell lines used, could reduce tumor cell migration. For example, Zhou *et al.* showed decreased chemotactic responses in transwell chamber when breast, prostate or skin cancer cells were exposed to gold nanorods[22]. More recently, Li *et al.* performed wound healing assays and demonstrated that gold nanospheres reduced liver cancer cells migration[33]. Similarly, time-lapse videomiscroscopy of wound healing of lung and prostate cancer cells has shown that gold nanospheres affect early cell migration (6 h) with decreased gap filling[34].

Au@DTDTPA(Gd) nanoparticles uptake affect the intrinsic biomechanical properties of glioma cells and cell-ECM interactions.

From a biomechanical standpoint, tumor cell motion in case of mesenchymal migration requires cell deformation and active generation of traction force on the underlying extracellular matrix to pull the cell forward. Cell deformation is directly dependent on the stiffness properties and the transition to a motile phenotype is characterized by changes in focal adhesion and cytoskeletal dynamics. Previous studies have reported a correlation between cell stiffness and metastatic potential of cancer cells[7] and that cancer cells are softer than normal cells[35]. Then, we have investigated the impact of Au@DTDTPA(Gd) on the deformability and stiffness of U251 by using AFM-indentation measurements and by the Young's modulus determination. In this case, isolated cell was selected out of a cell culture on fibronectin coated coverslip and AFM measurements were realized in areas outside the nucleus, where the cell height was at least 3 times superior to the indentation depth in order to calculate the Young's modulus. The Young's modulus was found to be remarkably stable on control cells with values equal to 1.61 ± 0.17 kPa. After Au@DTDTPA(Gd) uptake, the Young's modulus dramatically increased to reach 4.56 ± 2.58 kPa on fibronectin (Figure 4A). Moreover, it is well documented that cell migration is dependent on lamellipodial protrusion[36]. Using AFM error images, we have analyzed the number of membrane protrusions and demonstrated that treatment with Au@DTDTPA(Gd) induced a decrease of about 50% in the protrusion number (5.30 ± 0.39 protrusions per 100 µm² for the control samples *vs* 2.43 ± 0.31 protrusions per

100 µm² for the treated cells) (Figure 4B). All these results highlighted the potential of NPs to diminish the capacities of U251 cells to displace.

In order to explain and correlate the increase in the Young's modulus and the decrease in the migration capabilities of U251 cells after Au@DTDTPA(Gd) treatments, fluorescently labeled phalloidin has been used to study actin cytoskeleton organization by confocal microscopy. Supporting information SI3 shows the 3D isosurface reconstruction of cells using 2 different thresholds for untreated control cells or nanoparticles-treated cells. At the lowest threshold (Figure 4C), a clear difference appears in the actin labeling between untreated and Au@DTDTPA(Gd)-treated cells. While only the actin cortex is visible in control cells, the Au@DTDTPA(Gd)-treated cells exhibit a well-developed intracellular stress fibers and thicker actin cortex. Adhesion structures appear clearly at the edge of U251 cells and actin patches with a highest threshold value (framed areas) are more present in nanoparticles-treated cells. Our observations corroborate previous published studies that reported changes in F-actin fibers organization when cells were exposed to inorganic nanoparticles[37]. More recently, Mulens-Arias *et al.* showed that AuNPs disturbed adhesive structures and affected focal adhesion dynamics, in particular, characterized by an increase or a decrease in mature focal adhesion in the first 2 h following exposure according to the type of cells studied (mesenchymal stem cells or endothelial cells, respectively). Nevertheless, the effects appear to be dependent on nanoparticles core size and cell type[38]. Consistently, we conducted further molecular investigations to determine how Au@DTDTPA(Gd) interfere with actin cytoskeletal system. Thus, we studied by immunoblotting membrane expression of beta 1 integrin from biotinylated extracts (Figure 4D and 4E) and expression of Talin-1 expression (Figure 4F). While no difference of total beta 1 integrin expression was noticed between untreated- and nanoparticles-treated cells, membrane expression of beta 1 integrin was doubled when U251 cells were exposed to 5 mM Au@DTDTPA(Gd) nanoparticles. In parallel, Talin-1 expression, an ubiquitous cytosolic protein that is found in high concentrations in focal adhesions, was markedly increased in Au@DTDTPA(Gd)-treated cells. These results evoke the stabilization of focal adhesion plaques in presence of nanoparticles, confirming the disturbance of focal adhesion dynamics[39].

To adhere and migrate, cells generate traction forces through the cytoskeleton[40]. So, using time-lapse traction force microscopy (TFM), we examined the differences in traction force generated by U251 cells pre-exposed or not to Au@DTDTPA(Gd) nanoparticles (movie 2). Traction force microscopy yields a spatial image of the stress exerted by cells on elastic gel substrates. As a cell attaches to the surface of the substrate, it deforms the substrate proportionally to the applied mechanical force and these elastic deformations can be followed by videomicroscopy and described quantitatively with high precision[41]. At a moderate stiffness mimicking conditions in healthy and tumor brain tissue (E = 5 to 15 kPa)[42], measurements of cellular force indicate that after 24 h exposure to Au@DTDTPA(Gd), U251 glioma cells exhibit stronger traction stresses compared to the non-exposed cells (Figure 5A and 5B) with force *ratio* reaching 13 410 ± 381 Pa/µm²) and 18 056 ± 616 Pa/µm² ($p = 0.0047$), respectively. These data confirm that nanoparticles accumulated into cell cytoplasm induce changes in force generation and corroborate previous data showing higher levels of cell traction force for TR146 epithelial cells that have been exposed to TiO_2 or SiO_2 nanoparticles while migrating collectively[43].

In order to reinforce the results obtained on cytoskeleton, stiffness and TFM, we finally focused our investigations on the direct adhesion properties of U251 cells by using a cell adhesion assay performed at 3 time points (15, 30

and 60 min) on a fibronectin or hyaluronic acid coating. As expected, in the control group, the percentage of attached cells increased over time, with a maximum reaching 24.8% and 27.8% for U251 plated on fibronectin and hyaluronic acid, respectively (Figure 5C and 5D). Regardless of the coating and the time points, pretreatment with Au@DTDTPA(Gd) conferred a significantly higher ability to adhere to the substrate. From 15 min of cell incubation with the matrix coating, 25.5 ± 1.7 % of U251 cells treated with nanoparticles bind to fibronectin, compared to only 12.6 ± 1.0 % of control cells ($p = 0.0043$). For U251 cells exposed to nanoparticles, adhesion at 60 min reached 42.2 ± 4.1 % compared to 23.8 ± 3.1 % for control cells ($p = 0.0159$). According to the images captured after 15 minutes (Figure 5E), the cytoskeleton appeared more developed for the Au@DTDTPA(Gd)-treated cells than for the control cells, which may explain the earlier and more important adhesion for the treated cells.

Taken together, our experiments demonstrated that Au@DTDTPA(Gd) uptake is able to counteract the migration capabilities of U251 glioma cells. These effects occur through an alteration of the intrinsic biomechanical behavior of cells that were characterized by an increase of Young's modulus, a reorganization of the actin cytoskeleton and adhesion structures, and higher traction forces. All these data are consistent with an enhanced anchorage of the cells after treatment with Au@DTDTPA(Gd) nanoparticles that likely explain the diminished capacities of collective and individual migration. Such effects of metal-based nanoparticles on cell motility seem to be generalized as some of them have already been observed for other inorganic nanoparticles and other cell types[22,33,38,43]. Our experiments have gone further as 3D invasion assays demonstrated that reduced motility of glioma cells also occur in a confined environment, reducing glioma invasive potential. Underlying mechanisms remain unclear and ongoing experiments are now devoted to decipher at the molecular level the action of Au@DTDTPA(Gd) nanoparticles on glioma cells.

Furthermore, Winckler's team has recently demonstrated that glioma cells emit thin ultralong membrane protrusions (called as tumor microtubes) which help them to invade and colonize healthy brain tissue and form a complex network that convey tumor resistance to standard treatment modalities such as radiotherapy[44,45]. In light of this recent knowledge, our results showing that Au@DTDTPA(Gd) nanoparticles can significantly affect the protrusion number emitted by cells appear particularly promising.

View Article Online
DOI: 10.1039/D0NR08936B

EXPERIMENTAL SECTION

Au@DTDTPA(Gd) nanoparticles and ICP-MS dosage of gold

The synthesis and characterization of the Au@DTDTPA(Gd) nanoparticles were described earlier[46,47] (Supporting information SI4).

For a typical preparation of these gold nanoparticles, $HAuCl_4 \cdot 3H_2O$ (200 mg, 51.10^{-5} mol) was placed in a 250 mL round-bottom flask and was dissolved with methanol (60 mL). In another flask, DTDTPA (256 mg, 50.10^{-5} mol), water (40 mL) and acetic acid (2 mL) were mixed. This solution containing DTDTPA was added to the gold salt solution under stirring. The mixture turned from yellow to orange. $NaBH_4$ (195 mg, 515 x 10^{-5} mol) dissolved in water (13.2 mL) was added to the gold-DTDTPA solution under stirring at room temperature. At the beginning of the $NaBH_4$ addition, the solution first became dark brown then a black flocculate appeared. The vigorous stirring was maintained for 1h before adding aqueous hydrochloric acid solution (2 mL, 1 M). After the partial removal of the solvent under reduced pressure the precipitate was retained on the polymer membrane and washed thoroughly and successively with 0.1 M hydrochloric acid, water and acetone. The resulting black powder was dried (up to 200 mg of dry powder of Au@DTDTPA) and dispersed in aqueous solution of sodium hydroxide (NaOH 0.01 M) to have a final concentration of 50 mM in gold.

The functionalization of Au@DTDTPA nanoparticles by organic dyes (aminated cyanine 3, Cy3-NH_2) was inspired from the grafting of aminated cyanine-5[21]. A solution of Au@DTDTPA (9 mL, 50 mM in gold) was adjusted at pH 5. For the activation of the carboxylic groups, EDC (397 mg) and NHS (477 mg) in deionized water (6.48 mL) were added to the colloid under stirring at room temperature. The agitation was maintained for 90 min. Afterwards, the pH of the solution was adjusted at pH 7.5 and Cy3-NH_2 was added to the aqueous suspension of Au@DTDTPA nanoparticles. The solution was stirred for 15 minutes at room temperature and for 12 h at 4°C.

After the reaction with Cy3-NH_2, the nanoparticles were purified by dialysis against acidic medium (pH 5, Molecular Weight Cut Off (MWCO): 6 kDa). The dialysis bath was changed four times (6 h, 20 h, 26 h, 40 h after the immersion of dialysis tube in acid aqueous solution) until it becomes colorless. After the purification by dialysis, the gold nanoparticles were concentrated by centrifugation using centrifugal concentrators (Vivaspin®, MWCO: 10 kDa) until a gold concentration of 50 mM.

Whatever the type of nanoparticles (Au@DTDTPA or fluorescent Au@DTDTPA nanoparticles), the labeling by gadolinium ions is performed through the addition of $GdCl_3$ to colloidal solution under stirring at room temperature. For a final gold concentration of 45 – 50 mM, the gadolinium concentration is 5 mM.

The titration of gold in colloids and in the cells were performed by ICP-OES analysis. The samples were first mineralized in ultrapure aqua regia to a final concentration of at least 20 µg/L in gold. An ICP-OES (710 ES Varian/Agilent) with axial torch with a concentric nebulizer and cyclonic spray chamber was used. The parameters fixed during measurement were: power of 1.2 kW with argon auxiliary of 1.5 L/min and nebulizer pressure of 200 kPa. The emission lines used to measure the gold concentration were 268 nm, 243 nm and 208 nm. The efficacy of the atomization is about 60% for gold. An ionizing buffer was employed for the measurements.

View Article Online
DOI: 10.1039/D0NR08936B

Cell culture

The human primary glioblastoma cell line U-251MG (Uppsala, Sweden) was obtained from American Type Culture Collection and was cultured in Dulbecco's modified Eagle's medium (DMEM) supplemented with 10% fetal bovine serum, 0.4% L-asparagine, 0.36% L-serine, 1% L-glutamine, 1% essential aminoacids, 0.5% non-essential amino acids, 0.4% vitamins, 1.25% sodium pyruvate, and 1% penicillin-streptomycin. Cells were maintained in monolayers in a tissue culture incubator at 37°C with a 5% CO2 95% air atmosphere, and were subcultured twice a week. DMEM, amino acids, vitamins, and antibiotics were purchased from Gibco/Life Technologies (France), while other reagents were obtained from Sigma-Aldrich (Saint Louis, MO, USA).

Cell counting was performed using TC20™ automated cell counter and viability assessment was determined using Trypan blue exclusion assay that allows the detection of live (unstained) and dead (stained) cells.

3D invasion assays

To generate U251 spheroids, 1.10^6 cells were plated in 75-cm² flasks previously coated with hydrophobic poly(2-hydroxyethyl methacrylate) to prevent cell adhesion. Four days later, small spheroids are harvested and placed in spinner culture flask with magnetic stirring for 10 days (U251MG cells) for growing. Then spheroid suspension was filtered through 380 and 520 µm mesh nylon filters that allowed collecting spheroids homogeneous in size (~ 400 – 500 µm). These later were then cultured in 6-well plates coated with poly(2-hydroxyethyl methacrylate) in presence or absence of 5 mM Au@DTDTPA(Gd) for 24 h. After treatment, each spheroid was placed into individual well of 96-well plate and then embedded with 100 µL of a mix of Matrigel® and hyaluronic acid (100 µg/mL). Spheroids were maintained at 37°C in a humidified 5% CO_2 atmosphere for 4 days, allowing invasion and migration processes to take place. After staining with thiazolyl blue tetrazolium bromide (MTT 1 mg/mL), invasion of viable cells was imaged using the GelCount® system (Oxford Optronix, UK). The mean area (in µm²) and the mean distance (in µm) of invasion from at least 34 independent spheroids (6 independent experiments) were quantified with Image J and GelCount® Software. Initial and end surface of spheroids (in µm²) from at least 19 independent spheroids (3 independent experiments) were quantified using Image J.

Wound healing assay

U251 glioblastoma cells were seeded at a concentration of $2.5.\ 10^5$ cells/well in 6-well plate containing Dulbecco's modified Eagle's medium culture medium supplemented with 10% fetal bovine serum (FBS) and incubated for 24h at 37°C in a humidified 5% CO_2 atmosphere. After attachment of the cells to the plate, cells were treated with 5 mM Au@DTDTPA(Gd) nanoparticles for 24 h. When nanoparticles were removed, a scratch was created into the confluent monolayer of U251 cells using a sterile p1000 pipet tip. The cells were then replaced into the incubator for 16h. Three representative images of each scratch area were captured at 0 h (just after scratching cells), and 16 h after incubation using a transmitted-light microscope (Nikon DIAPHOT 300 equipped with digital camera Nikon Digital sight-DS-Fi1) (40X magnification). The plugin "MRI Wound Healing Tool" from ImageJ helped us to determine the area of the gaps for each image. As an indicator of collective migration ability, the wound healing rate was calculated as following: $(Area_{0h} – Area_{16h})/Area_{0h}$ x100.

View Article Online
DOI: 10.1039/D0NR08936B

Cell tracking by time-lapse videomicroscopy imaging

U251 cells (1.10^4) were seeded on fibronectin-coated 24-well plate, allowed to attach to the substrate and treated with 5 mM Au@DTDTPA(Gd) nanoparticles during 24 h. Before imaging, cells were treated with 1 µg/mL mitomycin C for 2h to inhibit cell proliferation. Cells were then PBS-washed and fresh medium was added. Cells were maintained at 37 °C under 5% CO_2 atmosphere in a temperature-controlled chamber (PECON) and then observed under a ×20 magnification objective during 24 h using a Zeiss Axio Observer (Carl Zeiss MicroImaging GmbH, Germany). Data were acquired using the MetaMorph software (Roper Scientific). Cell velocity, distance and directional persistence analyses were computed using ImageJ software (National Institutes of Health, Bethesda, MD, USA). For each condition, 48 random-chosen cells have been tracked.

Atomic force microscopy imaging

Prior to AFM analyses, 5.10^5 U251 cells were seeded onto 50 mm willCo-dish® pre-coated with 10 µg/mL fibronectin. On the next day, cells were treated with 5 mM Au@DTDTPA(Gd) nanoparticles during 24h. Cells were washed with PBS before adding 2 mL of medium. Then, AFM measurements were performed with a Bioscope Catalyst™ (Bruker, Billerica, USA) mounted on a Nikon Eclipse Ti inverted microscope (Nikon, Tokyo, Japan) and operated in PFQNM mode to acquire topographical and mechanical images on live cells. This mode has proved itself to allow higher resolution at faster acquisition speed (similar to tapping mode imaging) than the classical Force-Volume measurements. Preliminary experiments have been achieved using SCANASYST-AIR probes (Bruker, Billerica, USA) having a nominal spring constant of 0.4 N/m and a resonance frequency of ~70 kHz but generally speaking, the cantilever was too stiff for this type of cells. This prompted us to utilize PFQNM-LC-A-CAL probes (Bruker, Billerica, USA), having a nominal spring constant of 0.1 N/m and a resonance frequency of ~45 kHz, the tips being calibrated as previously described. The tip geometry ("ace of spades" pyramidal shape, with a tip height of 17 µm and an apex diameter of approximately 130 nm) is designed on purpose to minimize the viscous drag during imaging in liquids. For PFQNM experiments, we used a PeakForce frequency of 0.25 kHz in order to maximize the contact time between the tip and the sample (and also collect more than one force curve per pixel), and a PeakForce amplitude of 1 µm to optimize the tracking since the cells are quite high (up to 7 µm). Images were captured in culture medium at a resolution of 256 or 128 pixels per line, at 37 °C using a Perfusing Stage Incubator (Bruker, Billerica, USA). The Petri dish was put on the baseplate when the temperature setpoint was reached and stable over time (a Lakeshore temperature controller was used). The Young's modulus, step height, surface and volume measurements were calculated using Nanoscope Analysis (Bruker, Billerica, USA). In the present study, only the surface density of protrusions and the cells mechanical properties were considered. With respect to the Young's modulus calculation, for each type of cells, 10 different cell dishes coming from the same culture were analyzed one after the other to avoid to work more than 3 h with each dish and the experiments were triplicated to draw a reliable conclusion. Overall, a minimum of 50 cells for each condition (with and without NP incubation) were analyzed. Considered both the indentation depth of the tip given by the deformation channel and the cell height given by the cross sections achieved on height images at the same locations, the Young's modulus was exclusively calculated in areas where the cell height was at least 3 times superior to the indentation depth, in order to avoid any influence of the substrate on the measured values. Thus, perinuclear areas were avoided. The Sneddon model was used to estimate the interaction between the tip and

the substrate. In order to avoid generating mechanical stress to the cells, the loading force was adjusted between a few tens up to a few hundreds of piconewtons. The force curves were extracted from chosen area from the PFQNM images using the Peak Force Capture option from the Nanoscope software. For the topographical AFM measurements (more in particular the cell protrusions, a minimum of 50 images was processed for each condition.

Immunocytofluorescence

U251 cells were plated at the density 5.10^3 cells/well in 8-well Labtek II coated with 10 µg/mL of fibronectin for one day. The cells were exposed to 5 mM of Au@DTDTPA(Gd) for 24 h. Cells were fixed with PFA 4% for 30 min, then gently washed three times with PBS. To visualize F-actin distribution, slides were incubated for 45 min with Alexafluor-488-conjugated phalloidin (Ab176753, Abcam) diluted 1/1000 in PBS with 2% (w/v) BSA. Cells were then washed three times with PBS. Immunofluorescence-labeled cell preparations were analyzed using a Zeiss LSM 710 confocal laser scanning microscope with the 63X oil-immersion objective zoom 1x and Zeiss operating system (Carl Zeiss MicroImaging GmbH, Deutschland). Acquisitions were performed by exciting Alexafluor 488 with Argon laser. Emitted fluorescence was detected through the appropriate wavelength window. Twenty images were captured with a 0.25 µm z-step.

Confocal and STED Microscopy

Confocal and STED Microscopy on immunostained U251 cells were performed using the STEDYCON (Abberior Instruments GmbH). Confocal microscopy was performed under pulsed excitation of Cy3 and Abberior STAR RED at 561 nm and 640 nm respectively, on samples mounted in Abberior mount liquid antifade (Abberior GmbH). STED depletion was performed using a pulsed 775 nm laser source. Image processing and analysis were performed in Image J.

Due to the high concentration of metallic nanoparticles in cells, STED observation could occasionally prove very difficult and use of high STED laser powers was precluded[48]. However, we managed to obtain comparison of STED and confocal on cells or cell regions at resolution of < 80 nm (and down to 50 nm) (Figure 1).

Proteins extraction and western-blot analysis

Whole-cell extracts were prepared as previously described[49]. Briefly, whole-cell extracts were prepared by scraping cells in ice-cold lysis buffer (10 mM Tris-HCl, pH 7.5, 150 mM NaCl, 5 mM EDTA, 1% Triton X-100, and proteinase inhibitor cocktail).

Cell surface protein isolation were performed as previously described[49]. After washing, cell surface proteins were biotinylated with PBS containing 0.5 µg/mL of EZ-Link sulfo-NHS-LC-biotin (Thermofisher) for 30 min at 4°C. After three washes, cells were incubated with 100 mM glycine for 30 min at 4°C in order to limit nonspecific binding. Cells were washed three times in ice-cold lysis buffer before protein extraction. Solubilized biotinylated proteins were then affinity purified using 40 µL of monomeric avidin-agarose beads (GE Healthcare, Chicago, IL, USA) incubated with 120 µg of biotinylated proteins. Incubation was performed overnight at 4°C under gentle orbital agitation (5 rpm), and then followed by five washes in lysis buffer.

The protein concentration in whole-cell extracts and membrane extracts was quantified by the Bradford method (Bio-Rad Laboratories, Marne-la-Vallée, France). Proteins were separated by sodium dodecyl sulfate-polyacrylamide gel electrophoresis, transferred onto a nitrocellulose membrane (Schleicher & Schuell GmbH, Mantes la Ville, France), and incubated overnight at 4°C with primary antibodies. Immunoreactive bands were revealed using an ECL Plus chemiluminescence kit from Amersham Biosciences (Orsay, France). GAPDH was used as a control to ensure equal loading.

Traction Force Microscopy

TFM requires three distinct procedures: (1) Cells are plated on an elastic substrate containing fiducial markers allowing to quantify gel deformation visually, for instance fluorescent beads or quantum dots. (2) A discrete gel displacement caused by adherent cells is calculated by tracking fluorescent beads movement. The most common techniques for tracking are particle image velocimetry (PIV) and particle tracking velocimetry (PTV). (3) Finally, the traction force field f is calculated from the displacement field by making use of a mechanical model of the elastic substrate[50].

Polyacrylamide gel coated coverslips were prepared at a 17 kPa modulus as previously described[51], using the following specific conditions: $1.5.10^5$ U251 cells were then seeded before adding 1 mM Au@DTDTPA(Gd)-Cy3 during 24 h.

Cells were washed twice and then observed under a ×63 objective using a Zeiss Axio Observer (Carl Zeiss MicroImaging GmbH) and a CoolSNAP HQ (Roper Scientific, France) camera. Image acquisitions were done every 5 min during 3 hours and beads displacement was analyzed using the JEasyTFM plugin runing under ImageJ.

Cell adhesion assay

6.10^4 U251 cells/mL were plated in 25-cm² flasks for 3 days. Then, tumor cells were treated with 5 mM Au@DTDTPA(Gd) for 24 h. In parallel, 48-well plates were pre-treated with 10 µg/ml of fibronectin or with 10 µg/ml hyaluronic acid in HBSS for 1 h at 37°C and then dried overnight at 4°C. Control or treated tumor cells were then stained with 1 mL Hoechst 33342 (20µM in HBSS, Thermo Scientific, 62249) for 30 min at 37°C and harvested. 1.10^5 stained cells/well were added on the pre-coated P48 plates. After 15, 30, and 60 min of incubation at 37°C in a humidified 5% CO_2 atmosphere, the cells were gently washed once with HBSS.

Measurement of attached cells after 15, 30, and 60 min. Washed cells were lysed with DMSO 100%. Quantification of fluorescence intensity of cell lysates (λexc/λem: 350 nm/461 nm) with a Tecan Infinite 200 microplate reader (Infinite M200 pro, Tecan™) allowed assessing attached cells for 7 independent experiments, each condition was realized in duplicate. To quantify the fluorescence at 0 min, 1.10^5 stained cells were transferred in 1,5 mL Eppendorf, then centrifugated at 300G during 10 min at 20°C. Supernatants were removed, then stained cells were lysed with DMSO 100%.

F-actin cytoskeleton of attached cells after 15 min. Au@DTDTPA(Gd) treatment and cell adhesion assay were conducted as previously described using Lab-Tek™ II Chamber Slide™ 8 wells coated with 10 µg/mL of fibronectin. 5.10^4 stained U251 cells were plated and after 15 min at 37°C in a humidified 5% CO_2 atmosphere, the cells were

View Article Online
DOI: 10.1039/D1NR08936B

gently washed once with HBSS. Cells were fixated with PFA 4% during 30 min, then gently washed once with PBS. F-Actin staining was performed using Alexafluor-488-conjugated phalloidin (Ab176753, Abcam) diluted 1/1000 in PBS with 2% (w/v) BSA. Phalloidin fluorescence was analyzed using an ImageXpress® Micro Confocal device with 10X Plan APO objective and MetaXpress Software (Molecular Devices, Sunnyvale, CA). Acquisitions were performed by exciting Alexafluor 488. Emitted fluorescence was detected through the appropriate wavelength window. Ten images were captured with a 1 µm z-step.

Statistical analysis

Mann-Whitney U test was used to compare untreated and treated groups. P-value less than 0.05 was considered as statistically significant.

View Article Online
DOI: 10.1039/D0NR08936B

CONCLUSION

Over the last decade, Roux *et al.* have developed the Au@DTDTPA(Gd) nanoparticles, *i.e.* original ultrasmall nanoparticles composed of a gold core and dithiolated polyaminocarboxylate shell doped with ~ 50 gadolinium ions, and demonstrated their relevance and their potential for MRI-guided radiation therapy[46,47]. In particular, preclinical experiments demonstrated that Au@DTDTPA(Gd) could be of interest for the management of brain tumor[5].

In the present work, exposure of U251 glioma cells to Au@DTDTPA(Gd) led into high accumulation of gold nanoparticles, that were mainly diffusely distributed in the cytoplasm of the tumor cells. Our results showed no direct *in vitro* cytotoxicity, and U251 cell proliferation was not altered. By contrast, our experiments pointed out a noticeable decrease in glioma cells invasiveness when tumor cells were exposed to Au@DTDTPA(Gd) nanoparticles. As the proteolysis activities were not directly affected by the intracytoplasmic accumulation of nanoparticles in our experimental conditions, the anti-invasive effect cannot be attributed to a matrix remodeling impairment. Instead, Au@DTDTPA(Gd) nanoparticles affected the intrinsic biomechanical properties of U251 glioma cells, such as cell stiffness, adhesion and generated traction forces, and significantly reduced the formation of protrusions, thus exerting an inhibitory effect on their migration capacities.

While initially developed for combining with radiation therapy, the Au@DTDTPA(Gd) nanoparticles could have huge interest for therapeutic management of astrocytic tumors, not only as radio-enhancing agent but also by reducing invasive potential of glioma cells. Indeed, it is well-established that migrating/invading glioblastoma cells preserve their stem-like properties with maintained tumorigenic potential[52] which makes anti-invasive strategies become a priority[53,54].

View Article Online
DOI: 10.1039/D0NR08936B

ACKNOWLEDGEMENTS

This work was supported by the research funds of (i) the Cancéropole Est, Régions Grand Est and Bourgogne-Franche-Comté, (ii) Ligue Contre le Cancer CCIR-GE, and (iii) the CPER. We would like to thank Adrien Dos Santos for his help for the graphical abstract. The authors thank Dr Christine Terryn of PICT platform for technical assistance in imaging.

REFERENCES

(1) Alieva, M.; Leidgens, V.; Riemenschneider, M. J.; Klein, C. A.; Hau, P.; van Rheenen, J. Intravital Imaging of Glioma Border Morphology Reveals Distinctive Cellular Dynamics and Contribution to Tumor Cell Invasion. *Sci Rep* **2019**, *9*. https://doi.org/10.1038/s41598-019-38625-4.

(2) Pinel, S.; Thomas, N.; Boura, C.; Barberi-Heyob, M. Approaches to Physical Stimulation of Metallic Nanoparticles for Glioblastoma Treatment. *Advanced Drug Delivery Reviews* **2019**, *138*, 344–357. https://doi.org/10.1016/j.addr.2018.10.013.

(3) Alric, C.; Miladi, I.; Kryza, D.; Taleb, J.; Lux, F.; Bazzi, R.; Billotey, C.; Janier, M.; Perriat, P.; Roux, S.; Tillement, O. The Biodistribution of Gold Nanoparticles Designed for Renal Clearance. *Nanoscale* **2013**, *5* (13), 5930–5939. https://doi.org/10.1039/C3NR00012E.

(4) McMahon, S. J.; Hyland, W. B.; Muir, M. F.; Coulter, J. A.; Jain, S.; Butterworth, K. T.; Schettino, G.; Dickson, G. R.; Hounsell, A. R.; O'Sullivan, J. M.; Prise, K. M.; Hirst, D. G.; Currell, F. J. Biological Consequences of Nanoscale Energy Deposition near Irradiated Heavy Atom Nanoparticles. *Scientific Reports* **2011**, *1*. https://doi.org/10.1038/srep00018.

(5) Miladi, I.; Alric, C.; Dufort, S.; Mowat, P.; Dutour, A.; Mandon, C.; Laurent, G.; Bräuer-Krisch, E.; Herath, N.; Coll, J.-L.; Dutreix, M.; Lux, F.; Bazzi, R.; Billotey, C.; Janier, M.; Perriat, P.; Duc, G. L.; Roux, S.; Tillement, O. The In Vivo Radiosensitizing Effect of Gold Nanoparticles Based MRI Contrast Agents. *Small* **2014**, *10* (6), 1116–1124. https://doi.org/10.1002/smll.201302303.

(6) Pernodet, N.; Fang, X.; Sun, Y.; Bakhtina, A.; Ramakrishnan, A.; Sokolov, J.; Ulman, A.; Rafailovich, M. Adverse Effects of Citrate/Gold Nanoparticles on Human Dermal Fibroblasts. *Small* **2006**, *2* (6), 766–773. https://doi.org/10.1002/smll.200500492.

(7) Arvizo, R. R.; Saha, S.; Wang, E.; Robertson, J. D.; Bhattacharya, R.; Mukherjee, P. Inhibition of Tumor Growth and Metastasis by a Self-Therapeutic Nanoparticle. *PNAS* **2013**, *110* (17), 6700–6705. https://doi.org/10.1073/pnas.1214547110.

(8) Li, W.; Li, X.; Liu, S.; Yang, W.; Pan, F.; Yang, X.-Y.; Du, B.; Qin, L.; Pan, Y. Gold Nanoparticles Attenuate Metastasis by Tumor Vasculature Normalization and Epithelial–Mesenchymal Transition Inhibition. *International Journal of Nanomedicine* **2017**, *12*, 3509. https://doi.org/10.2147/IJN.S128802.

(9) Chithrani, B. D.; Ghazani, A. A.; Chan, W. C. W. Determining the Size and Shape Dependence of Gold Nanoparticle Uptake into Mammalian Cells. *Nano Lett.* **2006**, *6* (4), 662–668. https://doi.org/10.1021/nl052396o.

(10) Chithrani, B. D.; Chan, W. C. W. Elucidating the Mechanism of Cellular Uptake and Removal of Protein-Coated Gold Nanoparticles of Different Sizes and Shapes. *Nano Lett.* **2007**, *7* (6), 1542–1550. https://doi.org/10.1021/nl070363y.

(11) Huang, K.; Ma, H.; Liu, J.; Huo, S.; Kumar, A.; Wei, T.; Zhang, X.; Jin, S.; Gan, Y.; Wang, P. C.; He, S.; Zhang, X.; Liang, X.-J. Size-Dependent Localization and Penetration of Ultrasmall Gold Nanoparticles in Cancer Cells, Multicellular Spheroids, and Tumors in Vivo. *ACS Nano* **2012**, *6* (5), 4483. https://doi.org/10.1021/nn301282m.

(12) Jiang, W.; Kim, B. Y. S.; Rutka, J. T.; Chan, W. C. W. Nanoparticle-Mediated Cellular Response Is Size-Dependent. *Nature Nanotechnology* **2008**, *3* (3), 145–150. https://doi.org/10.1038/nnano.2008.30.

(13) Chithrani, D. B.; Jelveh, S.; Jalali, F.; van Prooijen, M.; Allen, C.; Bristow, R. G.; Hill, R. P.; Jaffray, D. A. Gold Nanoparticles as Radiation Sensitizers in Cancer Therapy. *Radiat Res* **2010**, *173* (6), 719–728. https://doi.org/10.1667/RR1984.1.

(14) Boyoglu, C.; He, Q.; Willing, G.; Boyoglu-Barnum, S.; Dennis, V. A.; Pillai, S.; Singh, S. R. Microscopic Studies of Various Sizes of Gold Nanoparticles and Their Cellular Localizations https://www.hindawi.com/journals/isrn/2013/123838/ (accessed Sep 21, 2020). https://doi.org/10.1155/2013/123838.

(15) Chuang, S.-M.; Lee, Y.-H.; Liang, R.-Y.; Roam, G.-D.; Zeng, Z.-M.; Tu, H.-F.; Wang, S.-K.; Chueh, P. J. Extensive Evaluations of the Cytotoxic Effects of Gold Nanoparticles. *Biochimica et Biophysica Acta (BBA) - General Subjects* **2013**, *1830* (10), 4960–4973. https://doi.org/10.1016/j.bbagen.2013.06.025.

(16) Xia, Q.; Huang, J.; Feng, Q.; Chen, X.; Liu, X.; Li, X.; Zhang, T.; Xiao, S.; Li, H.; Zhong, Z.; Xiao, K. Size- and Cell Type-Dependent Cellular Uptake, Cytotoxicity and in Vivo Distribution of Gold Nanoparticles. *International Journal of Nanomedicine* **2019**, *14*, 6957. https://doi.org/10.2147/IJN.S214008.

(17) Hou, Y.; Cai, K.; Li, J.; Chen, X.; Lai, M.; Hu, Y.; Luo, Z.; Ding, X.; Xu, D. Effects of Titanium Nanoparticles on Adhesion, Migration, Proliferation, and Differentiation of Mesenchymal Stem Cells. *International Journal of Nanomedicine* **2013**, *8*, 3619. https://doi.org/10.2147/IJN.S38992.

(18) Fayzullin, A.; Sandberg, C. J.; Spreadbury, M.; Saberniak, B. M.; Grieg, Z.; Skaga, E.; Langmoen, I. A.; Vik-Mo, E. O. Phenotypic and Expressional Heterogeneity in the Invasive Glioma Cells. *Translational Oncology* **2019**, *12* (1), 122. https://doi.org/10.1016/j.tranon.2018.09.014.

(19) Vinci, M.; Box, C.; Eccles, S. A. Three-Dimensional (3D) Tumor Spheroid Invasion Assay. *J Vis Exp* **2015**, No. 99. https://doi.org/10.3791/52686.

(20) Tevis, K. M.; Colson, Y. L.; Grinstaff, M. W. Embedded Spheroids as Models of the Cancer Microenvironment. *Advanced Biosystems* **2017**, *1* (10), 1700083. https://doi.org/10.1002/adbi.201700083.

(21) Jiménez Sánchez, G.; Maury, P.; Stefancikova, L.; Campion, O.; Laurent, G.; Chateau, A.; Bouraleh Hoch, F.; Boschetti, F.; Denat, F.; Pinel, S.; Devy, J.; Porcel, E.; Lacombe, S.; Bazzi, R.; Roux, S. Fluorescent Radiosensitizing Gold Nanoparticles. *International Journal of Molecular Sciences* **2019**, *20* (18), 4618. https://doi.org/10.3390/ijms20184618.

(22) Zhou, T.; Yu, M.; Zhang, B.; Wang, L.; Wu, X.; Zhou, H.; Du, Y.; Hao, J.; Tu, Y.; Chen, C.; Wei, T. Inhibition of Cancer Cell Migration by Gold Nanorods: Molecular Mechanisms and Implications for Cancer Therapy. *Advanced Functional Materials* **2014**, *24* (44), 6922–6932. https://doi.org/10.1002/adfm.201401642.

(23) Shin, S.-S.; Noh, D.-H.; Hwang, B.; Lee, J.-W.; Park, S. L.; Park, S.-S.; Moon, B.; Kim, W.-J.; Moon, S.-K. Inhibitory Effect of Au@Pt-NSs on Proliferation, Migration, and Invasion of EJ Bladder Carcinoma Cells: Involvement of Cell Cycle Regulators, Signaling Pathways, and Transcription Factor-Mediated MMP-9 Expression. *International Journal of Nanomedicine* **2018**, *13*, 3295. https://doi.org/10.2147/IJN.S158463.

(24) Cuddapah, V. A.; Robel, S.; Watkins, S.; Sontheimer, H. A Neurocentric Perspective on Glioma Invasion. *Nature reviews. Neuroscience* **2014**, *15* (7), 455. https://doi.org/10.1038/nrn3765.

(25) Roomi, M. W.; Kalinovsky, T.; Niedzwiecki, A.; Rath, M. Modulation of UPA, MMPs and Their Inhibitors by a Novel Nutrient Mixture in Human Glioblastoma Cell Lines. *International Journal of Oncology* **2014**, *45* (2), 887–894. https://doi.org/10.3892/ijo.2014.2465.

(26) Forsyth, P. A.; Wong, H.; Laing, T. D.; Rewcastle, N. B.; Morris, D. G.; Muzik, H.; Leco, K. J.; Johnston, R. N.; Brasher, P. M. A.; Sutherland, G.; Edwards, D. R. Gelatinase-A (MMP-2), Gelatinase-B (MMP-9) and Membrane Type Matrix Metalloproteinase-1 (MT1-MMP) Are Involved in Different Aspects of the Pathophysiology of Malignant Gliomas. *British Journal of Cancer* **1999**, *79* (11–12), 1828. https://doi.org/10.1038/sj.bjc.6990291.

(27) Liu, F.; Ma, D.; Chen, W.; Chen, X.; Qian, Y.; Zhao, Y.; Hu, T.; Yin, R.; Zhu, Y.; Zhang, Y.; Zhang, Y.; Zhao, W. Gold Nanoparticles Suppressed Proliferation, Migration, and Invasion in Papillary Thyroid Carcinoma Cells via Downregulation of CCT3 https://www.hindawi.com/journals/jnm/2019/1687340/ (accessed Sep 21, 2020). https://doi.org/10.1155/2019/1687340.

(28) Hagemann, C.; Anacker, J.; Ernestus, R.-I.; Vince, G. H. A Complete Compilation of Matrix Metalloproteinase Expression in Human Malignant Gliomas. *World Journal of Clinical Oncology* **2012**, *3* (5), 67. https://doi.org/10.5306/wjco.v3.i5.67.

(29) Rao, J. S. Molecular Mechanisms of Glioma Invasiveness: The Role of Proteases. *Nature Reviews Cancer* **2003**, *3* (7), 489–501. https://doi.org/10.1038/nrc1121.

(30) Friedl, P.; Wolf, K. Tumour-Cell Invasion and Migration: Diversity and Escape Mechanisms. *Nature Reviews Cancer* **2003**, *3* (5), 362–374. https://doi.org/10.1038/nrc1075.

(31) Jonkman, J. E. N.; Cathcart, J. A.; Xu, F.; Bartolini, M. E.; Amon, J. E.; Stevens, K. M.; Colarusso, P. An Introduction to the Wound Healing Assay Using Live-Cell Microscopy. *Cell Adhesion & Migration* **2014**, *8* (5), 440–451. https://doi.org/10.4161/cam.36224.

(32) Jain, P.; Worthylake, R. A.; Alahari, S. K. Quantitative Analysis of Random Migration of Cells Using Time-Lapse Video Microscopy. *J Vis Exp* **2012**, No. 63. https://doi.org/10.3791/3585.

(33) Li, L.; Zhang, W.; Seshadri, V. D. D.; Cao, G. Synthesis and Characterization of Gold Nanoparticles from Marsdenia Tenacissima and Its Anticancer Activity of Liver Cancer HepG2 Cells. *Artificial Cells, Nanomedicine, and Biotechnology* **2019**, *47* (1), 3029–3036. https://doi.org/10.1080/21691401.2019.1642902.

(34) Shahhoseini, E.; Feltis, B. N.; Nakayama, M.; Piva, T. J.; Pouniotis, D.; Alghamdi, S. S.; Geso, M. Combined Effects of Gold Nanoparticles and Ionizing Radiation on Human Prostate and Lung Cancer Cell Migration. *International Journal of Molecular Sciences* **2019**, *20* (18), 4488. https://doi.org/10.3390/ijms20184488.

(35) Xu, J.; Galvanetto, N.; Nie, J.; Yang, Y.; Torre, V. Rac1 Promotes Cell Motility by Controlling Cell Mechanics in Human Glioblastoma. *Cancers* **2020**, *12* (6), 1667. https://doi.org/10.3390/cancers12061667.

(36) Pontes, B.; Monzo, P.; Gole, L.; Le Roux, A.-L.; Kosmalska, A. J.; Tam, Z. Y.; Luo, W.; Kan, S.; Viasnoff, V.; Roca-Cusachs, P.; Tucker-Kellogg, L.; Gauthier, N. C. Membrane Tension Controls Adhesion Positioning at the Leading Edge of Cells. *J Cell Biol* **2017**, *216* (9), 2959–2977. https://doi.org/10.1083/jcb.201611117.

(37) Septiadi, D.; Crippa, F.; Moore, T. L.; Rothen-Rutishauser, B.; Petri-Fink, A. Nanoparticle–Cell Interaction: A Cell Mechanics Perspective. *Advanced Materials* **2018**, *30* (19), 1704463. https://doi.org/10.1002/adma.201704463.

(38) Mulens-Arias, V.; Balfourier, A.; Nicolás-Boluda, A.; Carn, F.; Gazeau, F. Disturbance of Adhesomes by Gold Nanoparticles Reveals a Size- and Cell Type-Bias. *Biomater. Sci.* **2018**, *7* (1), 389–408. https://doi.org/10.1039/C8BM01267A.

(39) Fang, K.-P.; Zhang, J.-L.; Ren, Y.-H.; Qian, Y.-B. Talin-1 Correlates with Reduced Invasion and Migration in Human Hepatocellular Carcinoma Cells. *Asian Pac J Cancer Prev* **2014**, *15* (6), 2655–2661. https://doi.org/10.7314/apjcp.2014.15.6.2655.

(40) Kraning-Rush, C. M.; Califano, J. P.; Reinhart-King, C. A. Cellular Traction Stresses Increase with Increasing Metastatic Potential. *PLOS ONE* **2012**, *7* (2), e32572. https://doi.org/10.1371/journal.pone.0032572.

(41) Plotnikov, S. V.; Sabass, B.; Schwarz, U. S.; Waterman, C. M. High-Resolution Traction Force Microscopy. *Methods Cell Biol* **2014**, *123*, 367–394. https://doi.org/10.1016/B978-0-12-420138-5.00020-3.

(42) Tanner, K. Perspective: The Role of Mechanobiology in the Etiology of Brain Metastasis. *APL Bioengineering* **2018**, *2* (3), 031801. https://doi.org/10.1063/1.5024394.

(43) Tay, C. Y.; Cai, P.; Setyawati, M. I.; Fang, W.; Tan, L. P.; Hong, C. H. L.; Chen, X.; Leong, D. T. Nanoparticles Strengthen Intracellular Tension and Retard Cellular Migration. *Nano Lett.* **2014**, *14* (1), 83–88. https://doi.org/10.1021/nl4032549.

(44) Osswald, M.; Jung, E.; Sahm, F.; Solecki, G.; Venkataramani, V.; Blaes, J.; Weil, S.; Horstmann, H.; Wiestler, B.; Syed, M.; Huang, L.; Ratliff, M.; Karimian Jazi, K.; Kurz, F. T.; Schmenger, T.; Lemke, D.; Gömmel, M.; Pauli, M.; Liao, Y.; Häring, P.; Pusch, S.; Herl, V.; Steinhäuser, C.; Krunic, D.; Jarahian, M.; Miletic, H.; Berghoff, A. S.; Griesbeck, O.; Kalamakis, G.; Garaschuk, O.; Preusser, M.; Weiss, S.; Liu, H.; Heiland, S.; Platten, M.; Huber, P. E.; Kuner, T.; von Deimling, A.; Wick, W.; Winkler, F. Brain Tumour Cells Interconnect to a Functional and Resistant Network. *Nature* **2015**, *528* (7580), 93–98. https://doi.org/10.1038/nature16071.

(45) Weil, S.; Osswald, M.; Solecki, G.; Grosch, J.; Jung, E.; Lemke, D.; Ratliff, M.; Hänggi, D.; Wick, W.; Winkler, F. Tumor Microtubes Convey Resistance to Surgical Lesions and Chemotherapy in Gliomas. *Neuro-Oncology* **2017**, *19* (10), 1316–1326. https://doi.org/10.1093/neuonc/nox070.

(46) Debouttière, P.-J.; Roux, S.; Vocanson, F.; Billotey, C.; Beuf, O.; Favre-Réguillon, A.; Lin, Y.; Pellet-Rostaing, S.; Lamartine, R.; Perriat, P.; Tillement, O. Design of Gold Nanoparticles for Magnetic Resonance Imaging. *Advanced Functional Materials* **2006**, *16* (18), 2330–2339. https://doi.org/10.1002/adfm.200600242.

(47) Alric, C.; Taleb, J.; Le Duc, G.; Mandon, C.; Billotey, C.; Le Meur-Herland, A.; Brochard, T.; Vocanson, F.; Janier, M.; Perriat, P.; Roux, S.; Tillement, O. Gadolinium Chelate Coated Gold Nanoparticles As Contrast Agents for Both X-Ray Computed Tomography and Magnetic Resonance Imaging. *J. Am. Chem. Soc.* **2008**, *130* (18), 5908–5915. https://doi.org/10.1021/ja078176p.

(48) Schloetel, J.-G.; Heine, J.; Cowman, A. F.; Pasternak, M. Guided STED Nanoscopy Enables Super-Resolution Imaging of Blood Stage Malaria Parasites. *Scientific Reports* **2019**, *9* (1), 4674. https://doi.org/10.1038/s41598-019-40718-z.

(49) Theret, L.; Jeanne, A.; Langlois, B.; Hachet, C.; David, M.; Khrestchatisky, M.; Devy, J.; Hervé, E.; Almagro, S.; Dedieu, S. Identification of LRP-1 as an Endocytosis and Recycling Receptor for β1-Integrin in Thyroid Cancer Cells. *Oncotarget* **2017**, *8* (45), 78614–78632. https://doi.org/10.18632/oncotarget.20201.

(50) Huang, Y.; Schell, C.; Huber, T. B.; Şimşek, A. N.; Hersch, N.; Merkel, R.; Gompper, G.; Sabass, B. Traction Force Microscopy with Optimized Regularization and Automated Bayesian Parameter Selection for Comparing Cells. *Scientific Reports* **2019**, *9* (1), 539. https://doi.org/10.1038/s41598-018-36896-x.

(51) Yeung, T.; Georges, P. C.; Flanagan, L. A.; Marg, B.; Ortiz, M.; Funaki, M.; Zahir, N.; Ming, W.; Weaver, V.; Janmey, P. A. Effects of Substrate Stiffness on Cell Morphology, Cytoskeletal Structure, and Adhesion. *Cell Motility* **2005**, *60* (1), 24–34. https://doi.org/10.1002/cm.20041.

(52) Munthe, S.; Sørensen, M. D.; Thomassen, M.; Burton, M.; Kruse, T. A.; Lathia, J. D.; Poulsen, F. R.; Kristensen, B. W. Migrating Glioma Cells Express Stem Cell Markers and Give Rise to New Tumors upon Xenografting. *J Neurooncol* **2016**, *130* (1), 53–62. https://doi.org/10.1007/s11060-016-2221-y.

(53) Broekman, M. L.; Maas, S. L. N.; Abels, E. R.; Mempel, T. R.; Krichevsky, A. M.; Breakefield, X. O. Multidimensional Communication in the Microenvirons of Glioblastoma. *Nature Reviews Neurology* **2018**, *14* (8), 482–495. https://doi.org/10.1038/s41582-018-0025-8.

(54) Vollmann-Zwerenz, A.; Leidgens, V.; Feliciello, G.; Klein, C. A.; Hau, P. Tumor Cell Invasion in Glioblastoma. *Int J Mol Sci* **2020**, *21* (6). https://doi.org/10.3390/ijms21061932.

View Article Online
DOI: 10.1039/D0NR08936B

Table 1: Quantification of gold in the U251 cells based on ICP-OES analysis.

U251 cells maintained as monolayer culture were exposed for 24h to Au@DTDTPA(Gd) at 1 or 5 mM. After nanoparticles removal, cells were rinsed, detached, counted and centrifugated to obtain a pellet. Samples were then mineralized and proceeded as described in Material and Method section.

Au@DTDTPA(Gd) concentration	Gold quantity (µg)	Nanoparticles per cell
1 mM	0.48 ± 0.042	$6.17.10^6 \pm 5.65.10^4$
5 mM	0.55 ± 0.037	$6.99.10^6 \pm 5.46.10^4$

View Article Online
DOI: 10.1039/D0NR08936B

FIGURE LEGENDS

Figure 1: Localization of Au@DTDTPA(Gd) nanoparticles in U251 cells. (A-D) To precise subcellular distribution of Au@DTDTPA(Gd) nanoparticles, confocal and STED microscopy experiments were conducted using Cyanine3-labeled Au@DTDTPA(Gd) (green fluorescence) and markers of particular compartments (red fluorescence): antibodies labelled with STAR RED were directed against **(A)** EEA1 for endosomes, **(B)** calnexin for rough endoplasmic reticulum, **(C)** vinculin for focal adhesion complexes and **(D)** CoxIV for mitochondria. Left panel: confocal overview of a fixed cell (scale bar 5 µm). A region delineated by dotted white rectangle was zoomed in for confocal (middle panel) or STED (right panel) (scale bar 2 µm). **(E)** Maximal image intensity in XY, XZ, and YZ sections through the U251 nuclei after Au@DTDTPA(Gd)-Cy3 exposure (1 mM). XY section shows one slice through the nucleus of a single U251 cell; XZ section shows a cut along the horizontal yellow line through the nucleus; YZ section shows a cut along the vertical yellow line. The white dotted line delineates the nucleus of the cell. The green fluorescence signal corresponds to Au@DTDTPA(Gd): only the nanoparticles that cross the given cut are visible. The green intensity profile indicates a strong accumulation of nanoparticles at the periphery of the nucleus as well as their presence to a lesser extent in the nucleus. **(F)** Based on Trypan blue exclusion assay and TC20™ automated cell counter, viable cells were determined in Control cell cultures (Ctrl) or 24 h after exposure to Au@DTDTPA(Gd) nanoparticles (1 mM or 5 mM). Results are presented as mean ± SD ($n \geq 4$).

Figure 2: Impact of Au@DTDTPA(Gd) nanoparticles on U251 invasiveness based on 3D invasion assay. U251 spheroids (~ 450 ± 70 µm in diameter) were exposed to 1- or 5-mM Au@DTDTPA(Gd) for 24 h. After nanoparticles removal, spheroids were seeded in 6-well culture plates (one spheroid per well) and each one was embedded in a mixture of Matrigel®, complete culture medium enriched with hyaluronic acid. **(A)** Using ImageJ software, the total area of invasion (manual yellow delineation) and the core area (white delineation) were determined 4 days after seeding for each spheroid, allowing to calculate the "invasion surface" (1 pixel = 10.58 µm). **(B)** Representative images of invasion for untreated- or Au@DTDTPA(Gd)-treated spheroids showed areas of collective (white arrows) and individual (black arrow) invasion. **(C)** Histograms represent the core growth (mm^2) and the invasion surface (mm^2) for untreated- or Au@DTDTPA(Gd)-treated spheroids. Results are presented as mean ± SD ($n \geq 11$ spheroids for at least $n \geq 3$ independent experiments). $^{**}p < 0.01$ according to the Mann-Whitney U test.

Figure 3: Impact of Au@DTDTPA(Gd) nanoparticles on collective and individual migration of U251 cells. (A and B) Collective migration of U251 glioma cells was assessed using wound healing assays. As soon as the nanoparticles were removed, a scratch was made into the confluent monolayer of U251 cells and **(A)** photographs (X40 magnification were captured immediately and 16 h after scratching. Representative images show the gap filling in control conditions (Ctrl) or after 24 h of exposure to 5 mM Au@DTDTPA(Gd) nanoparticles. **(B)** The plugin "MRI wound healing assay tool" from ImageJ software was used to measure the gap area at 0 h and 16 h, and calculate the wound healing rates as plotted on histograms. Results are presented as mean ± SD ($n = 8$ independent experiments).

(C-E) Individual migration was monitored by videomicroscopy. After seeding on fibronectin-coated coverslip, 48 untreated or nanoparticles-treated cells were individually tracked for 24 h by videomicroscopy (X20 *magnification* objective, using a Zeiss Axio Observer). Histograms represent **(C)** accumulated distance **(D)** euclidean distance **(E)** and velocity. Results are presented as mean ± SD. **p < 0.01 and ****p < 0.0001 according to the Mann-Whitney U test.

Figure 4: Impact of Au@DTDTPA(Gd) nanoparticles on biomechanical and cell morphology of U251 cells. (A-B) AFM measurements were performed to assess the surface density of protrusions and the cells mechanical properties (characterized by the Young's modulus) of U251 cells treated or not with Au@DTDTPA(Gd). A minimum of 50 cells for each condition were analyzed. **(A)** Young's Modulus and **(B)** number of protrusions per 100 µm² were plotted on histograms. **(C)** Representative z-stack images of F-actin cytoskeleton (Alexa Fluor™ 488 Phalloidin) obtained by confocal microscopy. **(D-E)** Effect of Au@DTDTPA(Gd) nanoparticles on membrane Beta 1 integrin expression. **(D)** Cell extracts were prepared from U251 biotinylated cells treated or not by 5 mM Au@DTDTPA(Gd) nanoparticles. Expression of Beta 1 integrin localized at the cell surface was analysed by 10% SDS-PAGE followed by western blotting. **(E)** Expression of Beta 1 integrin was quantified by densitometry and results are representative of three independent experiments and expressed as mean ± SD relative to the control (100%). **(F)** Effect of Au@DTDTPA(Gd) nanoparticles on Talin-1 (full size) expression. Cell extracts were prepared from U251 cells treated or not by 5 mM Au@DTDTPA(Gd) nanoparticles. Expression of Talin-1 was analysed by 10% SDS-PAGE followed by western blotting.

Figure 5: Impact of Au@DTDTPA(Gd) nanoparticles on traction forces and adhesion. (A) Representative snapshots of TFM analysis of single cells with the force represented as magnitude of control cells (left) and Au@DTDTPA(Gd) nanoparticles-treated cells (right) superimposed with the cell segmentation used for the force integration. **(B)** Force ratio (in pN/µm²) corresponding to the integration of the force values over the surface obtained by the segmentation of untreated- and nanoparticles-treated U251 cells and normalized by the surface value. **(C and D)** After 24 h of exposure to 5 mM Au@DTDTPA(Gd) nanoparticles, U251 cells were exposed to Hoechst 33342 at 1/1000 during 15 minutes. Then, cells were trypsinated and plated on 48 wells plates coated with **(C)** fibronectin or **(D)** hyaluronic acid during 15, 30 and 60 minutes. Fluorescence intensities (λexc/λem: 350/461nm for Hoechst 33342) were recorded. Histograms represent the percentage of cells that have adhered after 15, 30 and 60 minutes. Results are presented as mean ± SD (n = 7 independent experiments). *p < 0.05 and **p < 0.01 according to the Mann-Whitney U test. **(E)** Representative images of attached cells on fibronectin-coated surface at the time point 15 min were captured for U251 cells treated or not by 5 mM Au@DTDTPA(Gd) nanoparticles (F-actin- green, cell nuclei- blue).

Figure 1

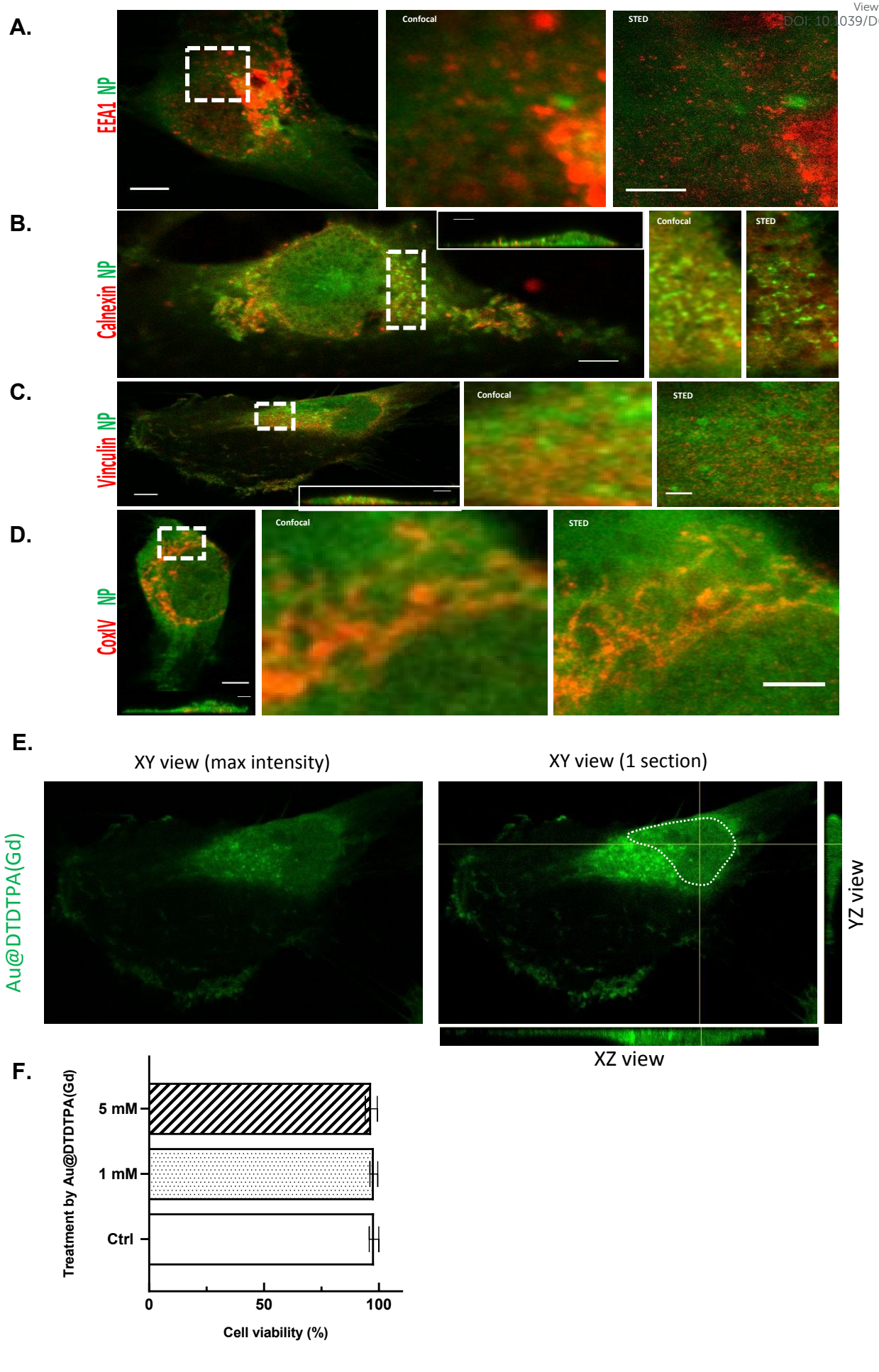

Figure 2

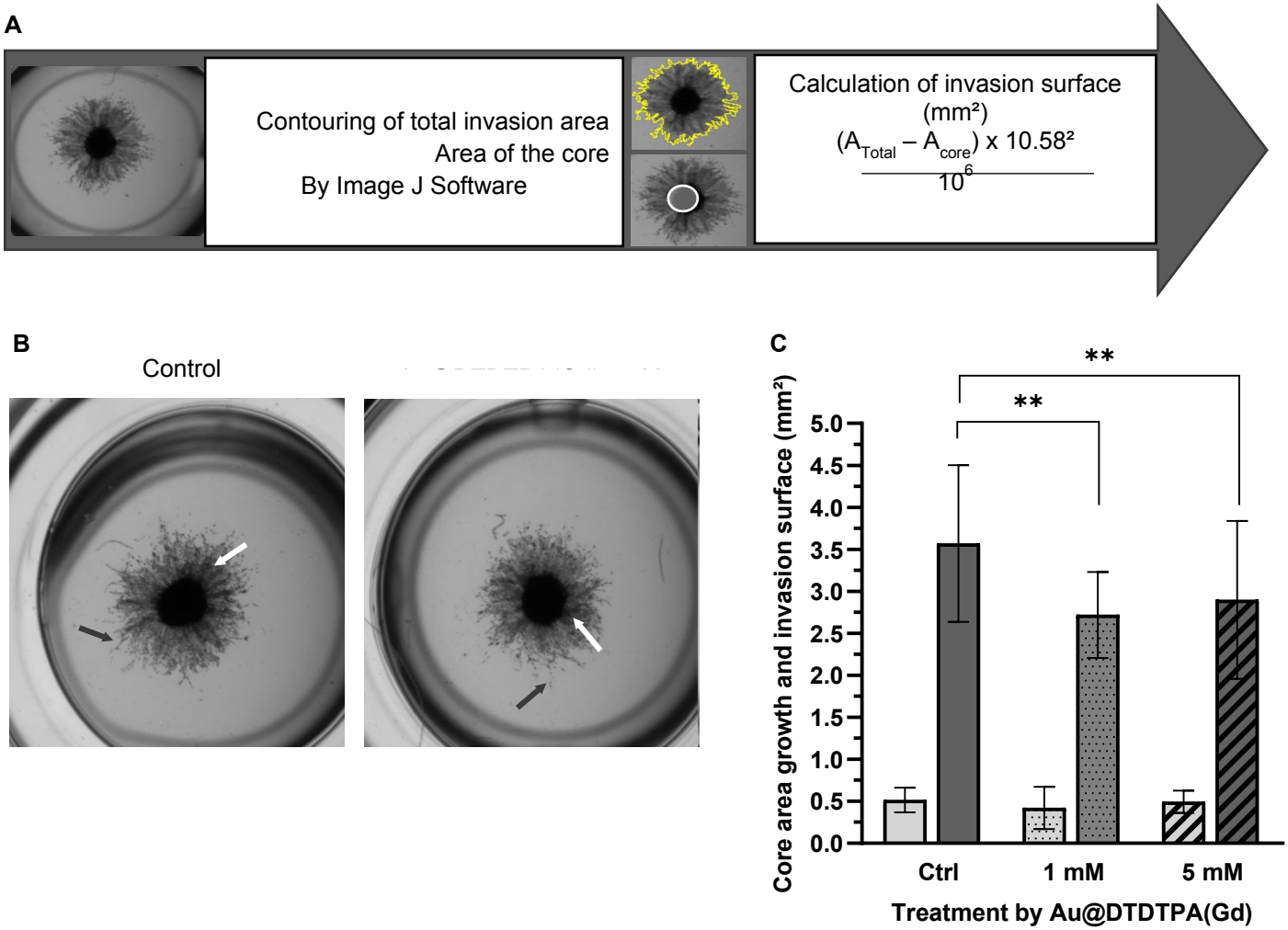

Figure 3

View Article Online
DOI: 10.1039/D0NR08936B

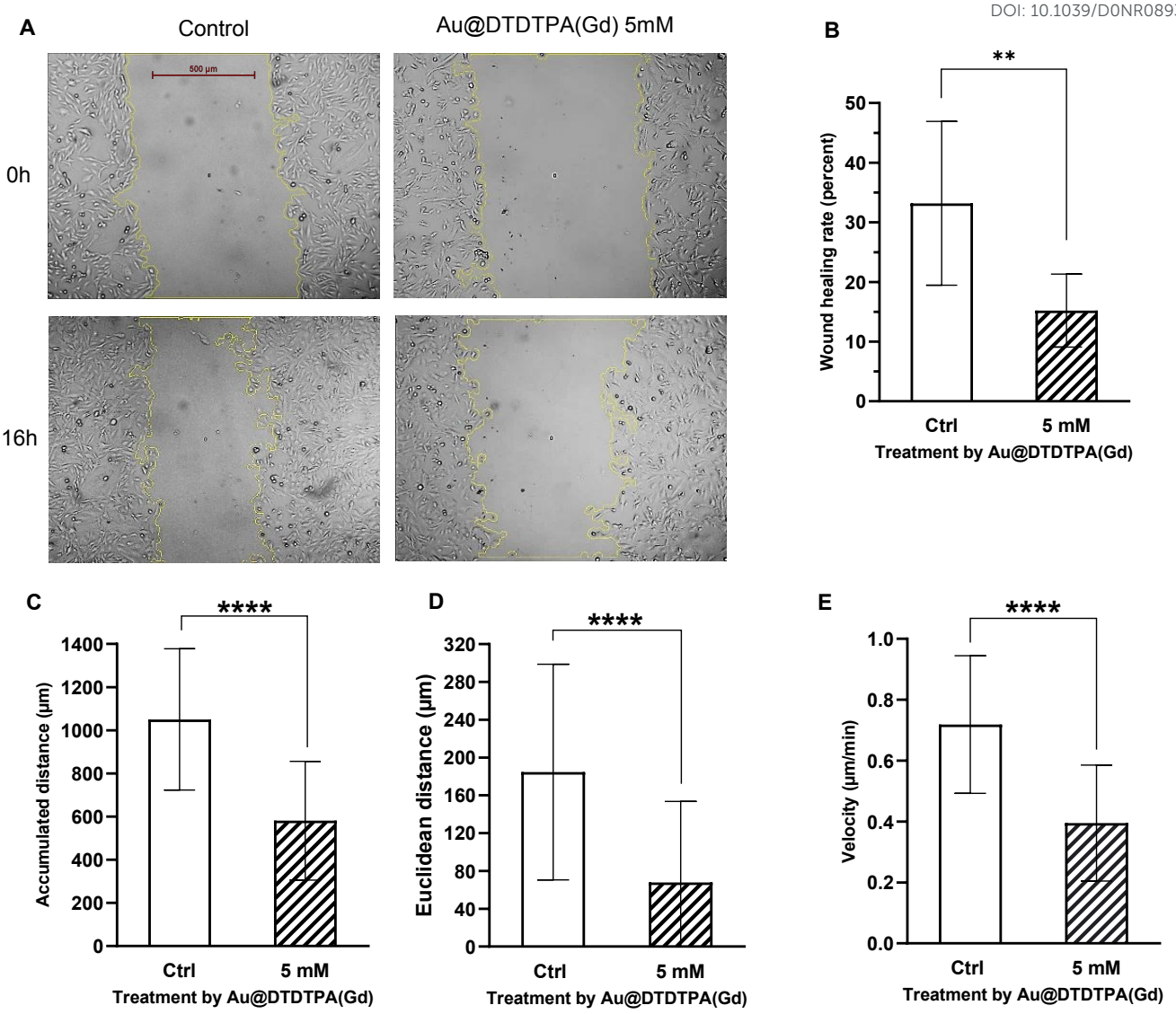

Figure 4

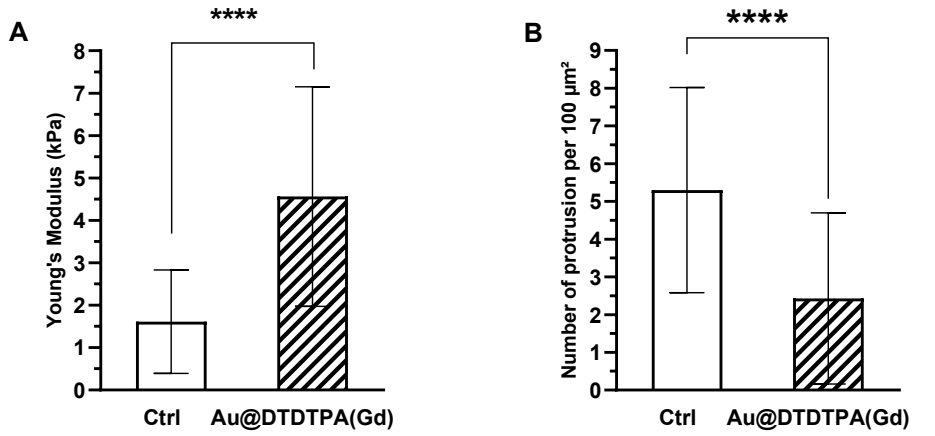

View Article Online
DOI: 10.1039/D0NR08936B

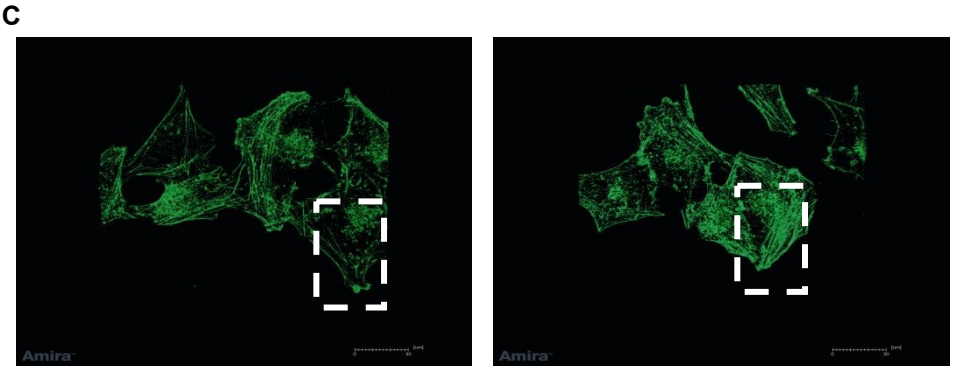

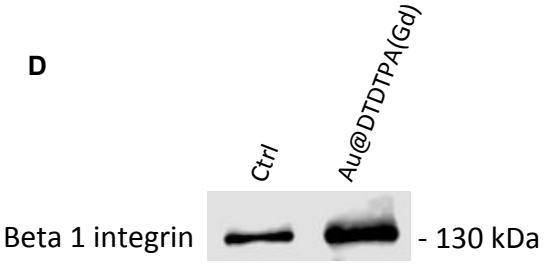

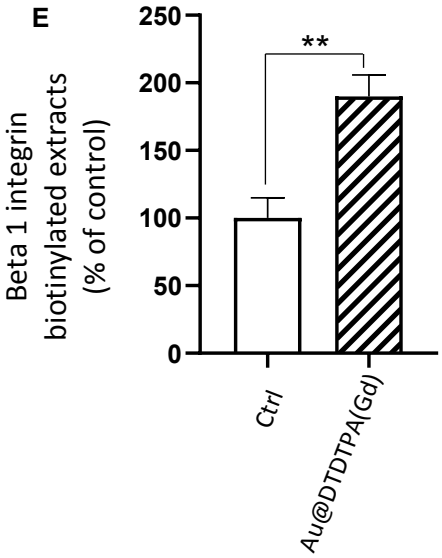

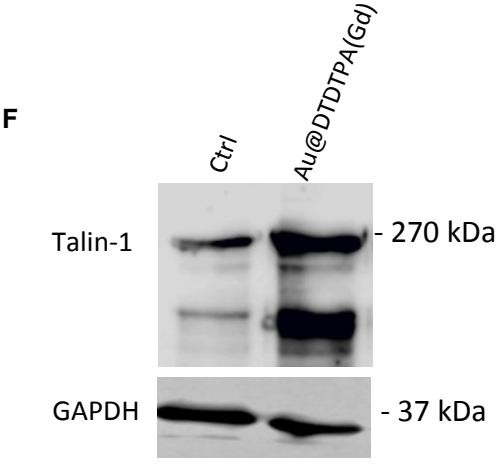

Figure 5

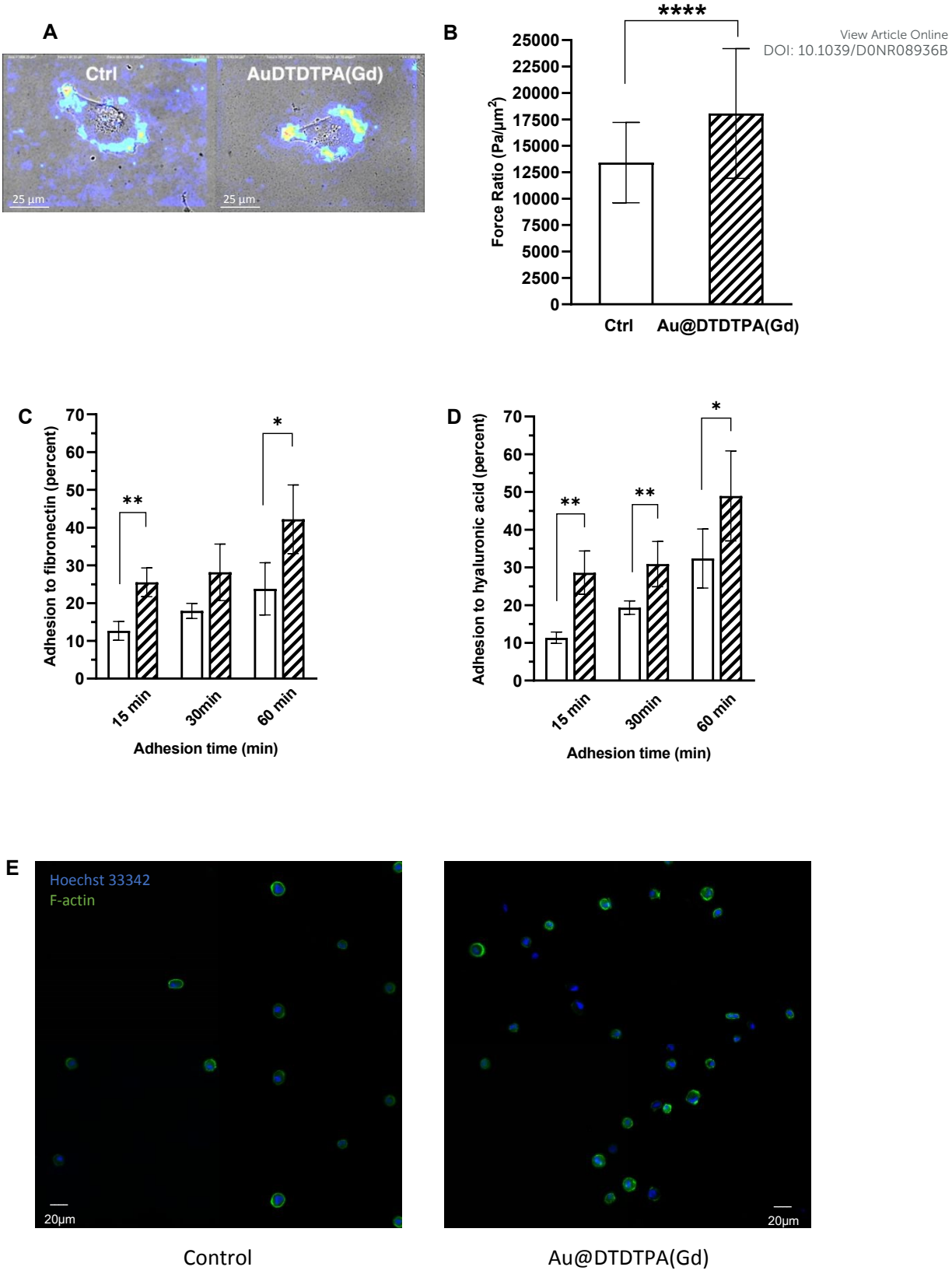

View Article Online
DOI: 10.1039/D0NR08936B